Remote Sens. **2014**, *6*, 5633-5649; doi:10.3390/rs6065633

OPEN ACCESS

remote sensing

ISSN 2072-4292

www.mdpi.com/journal/remotesensing

Article

Remote Sensing Assessment of Forest Disturbance across Complex Mountainous Terrain: The Pattern and Severity of Impacts of Tropical Cyclone Yasi on Australian Rainforests

Robinson I. Negrón-Juárez [1,2,*], Jeffrey Q. Chambers [1], George C. Hurtt [3], Bachir Annane [4], Stephen Cocke [5], Mark Powell [6], Michael Stott [7], Stephen Goosem [7], Daniel J. Metcalfe [8] and Sassan S. Saatchi [9]

[1] Climate Sciences Department, Earth Sciences Division, Lawrence Berkeley National Laboratory, 1 Cyclotron Rd., MS 50-4037, Berkeley, CA 94720, USA; E-Mail: jchambers@lbl.gov

[2] Department of Ecology and Evolutionary Biology, Tulane University, 6489 Saint Charles Av., New Orleans, LA 70118, USA

[3] Department of Geographical Sciences, University of Maryland, 2181 LeFrak Hall, College Park, MD 20742, USA; E-Mail: gchurtt@umd.edu

[4] Cooperative Institute for Marine and Atmospheric Studies (CIMAS), University of Miami, Coral Gables, FL 33149, USA; E-Mail: Bachir.Annane@noaa.gov

[5] Center for Ocean-Atmospheric Prediction Studies (COAPS), Florida State University, 2035 E. Paul Dirac Dr., 200 RM Johnson Bldg., Tallahassee, FL 32306, USA; E-Mail: scocke@fsu.edu

[6] Hurricane Research Division, National Oceanic and Atmospheric Administration, 4301 Rickenbacker Causeway, Miami, FL 33149, USA; E-Mail: Mark.Powell@noaa.gov

[7] Wet Tropics Management Authority, 1st Floor, Cairns Corporative Tower, 15 Lake St., P.O. Box 2050, Cairns, QLD 4870, Australia; E-Mails: mike.stott@wtma.qld.gov.au (M.S.); steve.goosem@wtma.qld.gov.au (S.J.)

[8] CSIRO Ecosystem Sciences–EcoSciences Precinct, 41 Boggo Road, Dutton Park, QLD 4102, Australia; E-Mail: dan.metcalfe@csiro.au

[9] Jet Propulsion Laboratory, California Institute of Technology, 4800 Oak Grove Drive, Pasadena, CA 91109, USA; E-Mail: Sasan.S.Saatchi@jpl.nasa.gov

* Author to whom correspondence should be addressed; E-Mail: robinson.inj@lbl.gov Tel.: +1-510-486-4000; Fax +1-510-486-5686.

Received: 29 January 2014; in revised form: 3 June 2014 / Accepted: 4 June 2014 / Published: 17 June 2014

Abstract: Topography affects the patterns of forest disturbance produced by tropical cyclones. It determines the degree of exposure of a surface and can alter wind characteristics. Whether multispectral remote sensing data can sense the effect of topography on disturbance is a question that deserves attention given the multi-scale spatial coverage of these data and the projected increase in intensity of the strongest cyclones. Here, multispectral satellite data, topographic maps and cyclone surface wind data were used to study the patterns of disturbance in an Australian rainforest with complex mountainous terrain produced by tropical cyclone Yasi (2011). The cyclone surface wind data (H*wind) was produced by the Hurricane Research Division of the National Oceanic and Atmospheric Administration (HRD/NOAA), and this was the first time that this data was produced for a cyclone outside of United States territory. A disturbance map was obtained by applying spectral mixture analyses on satellite data and presented a significant correlation with field-measured tree mortality. Our results showed that, consistent with cyclones in the southern hemisphere, multispectral data revealed that forest disturbance was higher on the left side of the cyclone track. The highest level of forest disturbance occurred in forests along the path of the cyclone track (±30°). Levels of forest disturbance decreased with decreasing slope and with an aspect facing off the track of the cyclone or away from the dominant surface winds. An increase in disturbance with surface elevation was also observed. However, areas affected by the same wind intensity presented increased levels of disturbance with increasing elevation suggesting that complex terrain interactions act to speed up wind at higher elevations. Yasi produced an important offset to Australia's forest carbon sink in 2010. We concluded that multispectral data was sensitive to the main effects of complex topography on disturbance patterns. High resolution cyclone wind surface data are needed in order to quantify the effects of topographic accelerations on cyclone related forest disturbances.

Keywords: multispectral data; complex mountainous terrain; tropical rainforests; tropical cyclones; forest disturbance

1. Introduction

Tropical cyclones (hurricanes, typhoons, and southern hemisphere cyclones) are recurrent weather phenomena responsible for fatalities, large economic losses [1] and are important drivers of the dynamics of forest ecosystems after landfall [2–4]. Tropical cyclones can produce changes in forest structure, biomass, species composition, nutrient regimes [4–7] and in the hydrological, energy, and carbon fluxes [4,8,9]. Although winds are responsible for most of the observed structural damage to forests from tropical cyclones, the severity of the impact also depends on biotic (e.g., tree size, species, and stand characteristics) and abiotic factors (e.g., soil type, topography and rainfall) [2,4,5,10] that operate at different spatial scales [11].

Regional-scale assessments of forest disturbance and recovery rely on the use of remote sensing data [12–16]. Studies based on field-measured tree mortality have confirmed that spectral reflectance

features vary with the level of cyclonic wind disturbance [8,9,17,18]. However, topographic characteristics play an important role in the pattern and severity of disturbance [11,18,19]. Topographic characteristics not only governs the degree of exposure of a forest to tropical cyclonic winds at any point [19] but can also alter both wind speed and direction [11] making the study of the association between terrain features and hurricane disturbance difficult.

Tropical rainforests are the most biodiverse biome in the world and play a major role in global hydrology, carbon storage, and climate [20]. They are also responsible for the highest carbon storage among all the world's forested ecosystems [21]. On 3 February 2011, Tropical Cyclone Yasi (hereafter referred to as Yasi) made landfall in northeast Queensland, Australia, as a Category 4 hurricane in the Saffir–Simpson Hurricane Scale [22]. Yasi was considered one of the most powerful cyclones to hit this region since 1918, with maximum wind gusts of about 285 km/h. The total economic loss resulting from Yasi was estimated at over 3 billion US dollars [23]. Yasi affected Australia's tropical rainforested areas that lie within the Wet Tropics of Queensland's World Heritage Area. These forests constitute a continuous mosaic of vegetation patches in various stages of recovery from previous cyclonic events [24]. In this study, remote sensing data, field-measured tree mortality, topographic maps and cyclone surface wind data are used to: (*i*) detail the sensitivity of multispectral data to forest disturbance in complex terrain; and, (*ii*) determine how terrain features influence the disturbance patterns. A coarse assessment of tree mortality associated with Yasi and a comparison of cyclone related disturbances using multispectral satellite data in tropical and temperate forests are also presented. This work presents the fundamentals of a recent complementary study [18].

2. Study Area and Dataset

2.1. Study Area

The study area is the northeastern rainforests of Queensland, Australia, affected by Yasi (Figure 1). These rainforests are part of the Wet Tropics of Queensland World Heritage Area (WTWHA), managed by the Wet Tropics Management Authority [25]. The WTWHA contains 900,000 ha of rainforest and is significant for its high diversity of primitive plant groups and large number of endemic species confined within its boundaries [26,27]. In this region the mean annual rainfall varies from 1200 mm to >3000 mm (a number of the higher summit areas can receive >8000 mm annually). Rainfall is seasonal with most falling during the summer wet season (December–March) [28]. Geology, landforms and flora are highly variable [28]. Broad parent geologies that can be found in this region include basalts, granites, metasediments and alluvium. Landforms include marine plains, salt pans, alluvial plains, low beach ridges, low hill, high hills, and mountains. Forests vegetation has an average height of 25–30 m and includes mesophyll, notophyll and microphyll rainforest types, tall open forests, open forests, woodlands and mangroves. Details about these forests are available on the Wet Tropics Management Authority website [25]. During the 2010–2011cyclone season, cyclones Tasha (landfall on 24 December 2010), and Anthony (landfall on 30 January 2011) also hit the Queensland region [23]. However, Tasha, characterized by weak winds, and Anthony (landfall ~250 km away from the area affected by Yasi) produced little to no effect on the forested areas affected by Yasi [23].

Figure 1. Hurricane Yasi track (dashed red line) and wind field (yellow isotachs). Wind classification follows the Saffir–Simpson Hurricane Scale: tropical storm (TS: 63–118 km/h (18–32 m/s)), hurricane category one (H1: 119–153 km/h (33–42 m/s)), hurricane category two (H2: 154–177 km/h (43–49 m/s)), hurricane category three (H3: 178–208 km/h (50–58 m/s)). The map also shows the tropical forested areas (Evergreen Broadleaf), in dark green, obtained using yearly land cover type data (L3 Global 500 m SIM Grid V051, MCD12Q1, Section 2.2). Ocean and water bodies are shown in black and land cover types other than tropical forests are shown in gray. The inlet shows the location of the study area.

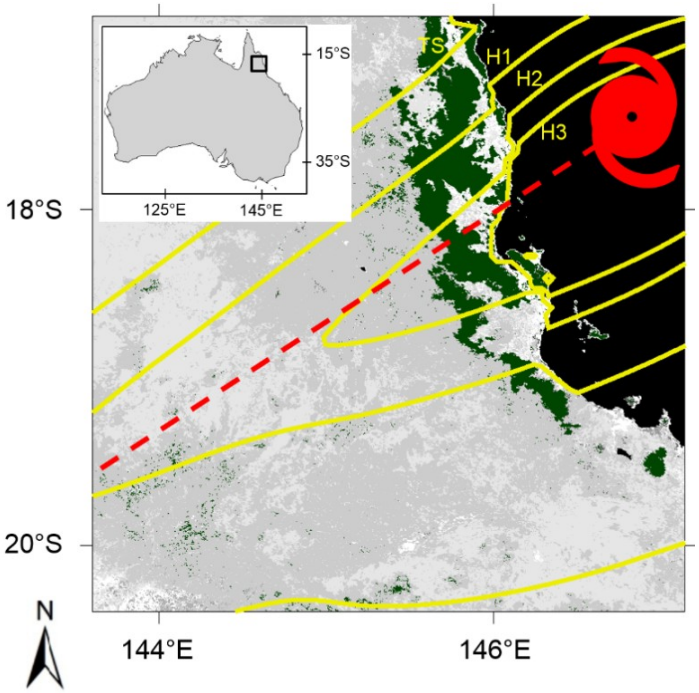

2.2. Yasi's Surface Wind Data

The Hurricane Research Division of the National Oceanic and Atmospheric Administration (HRD/NOAA) provided the surface wind fields associated with Yasi. The wind fields were based on objectively analyzing a blend of observations and a hurricane wind field model, that were then objectively analyzed using the HRD Real-time Hurricane Wind Analysis System (H*wind) [29,30]. The analysis resulted in maximum sustained one minute wind speeds and direction at 10 m above surface at ~5 km pixel resolution. Time stepping the appropriate field along the Australian Bureau of Meteorology storm track of Yasi at five minute intervals was used to construct hourly wind field snapshots and a wind swath. Accordingly, each grid point contains the maximum wind speed and its associated direction during the life of the storm at that point. It is worth mentioning that this is the first time that the H*wind model has been used for a southern hemisphere tropical cyclone since HRD/NOAA produces this data exclusively for the USA. Yasi H*Wind data is available at [31].

2.3. Multispectral Data

Optical remote sensing data from Vexcel UltraCam D (pixel size of 0.5 m), Landsat (30 m) and Moderate Resolution Imaging Spectroradiometer (MODIS, 500 m) were used in this study.

Vexcel UltraCam D (hereafter referred as Vexcel) scenes, mounted on an aircraft that flew between 760 to 1500 m asl (above sea level), produces images of 3680 × 2400 pixels in four spectral bands (blue, 410–540 nm; green, 480–630 nm; red, 580–700 nm; and NIR, 690–1000 nm) in Universal Transverse Mercator (UTM) geographic coordinate system, Zone 55 [32–34]. For the present study four Vexcel scenes (in the sector 8062 as designed by [33]) before and after Yasi were composed and served to identify potential research areas for field work. These four images were collected between 22 July and 4 August 2008 and 13–22 June 2011. Landsat 5 Thematic Mapper scenes (path 95 row 72) on 17 July 2009 and 22 July 2011 were also used. Finally, for a regional assessment of tree mortality this study used the MODIS surface reflectance data (MOD09A1, version 5-V005) [35] on 5 August 2010 and 5 August 2011. MOD09A1 provides seven bands of surface reflectance at 500-metre resolution in an 8-day gridded level-3 (L3) product in the Sinusoidal (SIN) projection. Only cloud- and shadow-free MOD09A1 pixels with no or only low cirrus clouds and affected by climatological or low aerosol were used.

MODIS/Terra+Aqua Land cover type yearly L3 Global 500 m SIM Grid V051 data (MCD12Q1) for 2010 was used to identify the forested pixels following the IGBP (International Geosphere-Biosphere Program) classification. MCD12Q1 pixels with good quality (Mandatory QA = 0) were used in this study. To cover the area affected by Yasi three MODIS scenes (h31v10, h31v11 and h32v10) were mosaicked and resampled to a Geographic Lat/Lon (WGS 84) projection using the MODIS Reprojection Tool (MRT). MOD09A1 bands were ordered as bands 3 (0.45–0.48 μm), 4 (0.54–0.56 μm), 1 (0.62–0.67 μm), 2 (0.84–0.87 μm), 6 (1.62–1.65 μm), and 7 (2.10–2.15 μm) in agreement with Landsat bands 1 (0.45–0.52 μm), 2 (0.52–0.60 μm), 3 (0.63–0.69 μm), 4 (0.76–0.90 μm), 5 (1.55–1.75 μm), and 7 (2.08–2.35 μm). The selection of images used in this study was influenced by characteristics of image availability and cloud-free images.

The pre-Yasi Landsat image was atmospherically corrected and converted to reflectance values using the Atmospheric Correction Now (ACORN) software (ImSpec LLC, Boulder, CO, USA). Visibility and water vapor parameters of the tropical atmospheric correction model available in ACORN were 40 mm and 100 km, respectively. Vexcel and Landsat Images were georeferenced using control points collected in the field and from around the Tully region of Queensland using a Global Positioning System device (Garmin GPSmap 60CSx). Vexcel and Landsat scenes were then converted to Geographic Lat/Lon (World Geodetic System-WGS 84) projection using ENVI software (Environment for Visualizing Images) (ITT Exelis, McLean, VA, USA). Vexcel and Landsat images post-Yasi were intercalibrated by regressing the encoded radiance against the respective pre-Yasi images using invariant targets (e.g., intact forest, bare soil, water, roads, cities) [17,36]. No intercalibration was performed in MOD09A1 data since the accuracy of this data has been ground-truth validated [35]. The images from Vexcel, Landsat and MODIS encompass the months of June, July and August, the dry season in the tropical areas of the Southern Hemisphere.

2.4. Topography Data and Carbon Map

The landforms in the area affected by Yasi were obtained from Global Multi-resolution Terrain Elevation Data 2010 (GMTED2010) at 15-arc-second (~500 m) spatial resolution. MRT, GMTED2010, MODIS and Landsat scenes are available at the Land Processes Distributed Active Center home page [37].

To assess the committed carbon release associated with Yasi we used the carbon storage per hectare over the area affected by this cyclone [21] (Figure S1).

3. Method

Spectral mixture analysis (SMA) [38] was applied on all images to quantify the severity of forest disturbance. SMA uses the spectral signature of endmembers, which sum to match the full pixel spectrum of the image, to determine the fraction of endmembers contained in each pixel [38]. During our field-assessments it was observed that the ground was mostly covered by fallen timber (associated with the high stem density, Figure S2) and surface vegetative litter. Consequently, bare soil did not constitute a significant fraction of the landscape. Since, SMA focus on the most representative ground surface elements [39] then soil endmember was not used. The image-derived endmembers considered were photosynthetic green vegetation (GV), non-photosynthetic vegetation (NPV), and shade. GV was obtained over the forested areas pre-Yasi. On the images, NPV was obtained from disturbed forests that were easily recognized due to their high values in the middle infrared reflectance band (e.g., MODIS band 6, 1.62–1.65 μm). These high values are due to the increased volumes of wood, dead vegetation, and surface litter exposed to the satellite sensor. The shade endmember was included to account for effects related to view angle, topography, shading, and shadows [39]. To select potential endmembers of GV, NPV and shade the pixel-purity-index, available in ENVI [40], was applied on boxes of 50 × 50 pixels. The potential endmember producing little or none of the other two endmembers [39] was selected as the final endmember. Pixels without the endmembers considered (for instance, land use areas, dirty roads, and bare soil) will not fit the SMA model and are easily identified by their large root mean square residual values [39]. Those pixels were excluded from the analysis. The fractions of GV and NPV were then normalized without shade as GV/(GV + NPV) and NPV/(GV + NPV) [39], hereafter referred to simply as GV and NPV. This procedure allows a direct comparison of fractions between the pre- and post-Yasi imagery. Change in NPV (ΔNPV) provides a quantitative measure of shifts in dead vegetation and woody biomass associated with disturbance [8], and was calculated by subtracting pre-Yasi NPV from post-Yasi NPV.

The high resolution of Vexcel images allowed us to identify strategic areas to perform our field study, to plan out the best track to follow (reducing time and effort) due to difficult access associated with the extent of fallen tree trunks and branches and to improve our logistics. Thus Vexcel images were extremely helpful in the Australian rainforest characterized by complex topography, dense forest and endemic and dangerous species (e.g., stinging tree, *Dendrocnide moroides*). The location of research plots were determined using Vexcel-ΔNPV maps. Forty-five plots (10 m × 10 m) were established in July 2012 along a 400 m transect which encompassed the entire gradient of disturbance regimes (from non-disturbed to severely disturbed forest), as well as the complex terrain from the windward to the leeward sides of mountains and valleys (see transect location in Figure 2). Our field validation was performed 17 months after Yasi made landfall. During this period no other cyclone affected the study area. Since trees in tropical forest take several years to decompose [41] the field data collection period post-Yasi that was used to validate the satellite disturbance metric associated with Yasi is realistic. Living and dead trees with diameters ≥10 cm at a height of 1.3 m above the ground (dbh) were counted at each plot. Dead trees are defined here as uprooted trees and the term mortality quantifies the number

of dead trees per unit area. The stem densities from these plots were combined with other published plot data from this region. This combined data set was used to derive a regional stem density of 408 to 1080 trees per hectare (Figure S2). The carbon stock map (Figure S1) was resampled to the 500 m pixel resolution to be consistent with MODIS Vegetation Type and MODIS-ΔNPV images. A Monte Carlo that simulation that included the uncertainties of used variables (scaling processes, stem density, and carbon map) calculated the total number of dead trees and the associated committed carbon emission using ten thousand interactions per MODIS pixel. The procedure is similar to that presented in [8].

Figure 2. (**a**) Relationship between field-measured mortality and ΔNPV. The linear regression (blue line), and the 95% confidence (solid red line) and prediction (dashed red line) bands are shown; (**b**) Forest disturbance severity (ΔNPV) for the Vexcel, Landsat and MODIS data used. The location of the 400 m × 10 m transect which covered the full range of disturbance values is shown in white in the inset in Vexcel image. Landsat ΔNPV and MODIS ΔNPV show the impact across the whole forested area affected by Yasi. ΔNPV was not calculated over forested areas affected by cloud cover (dark grey in Landsat and dark green in MODIS) in either pre or post Yasi images. In the MODIS scene, ocean and water bodies are shown in black and land cover types other than tropical forests are shown in intensities of gray obtained using MCD12Q1. Yasi wind intensities (Figure 1) are shown in dashed lines. For a comparison of the regional impact of Yasi on tropical forested areas, see Figure 1. Data in (**b**) partially after [18].

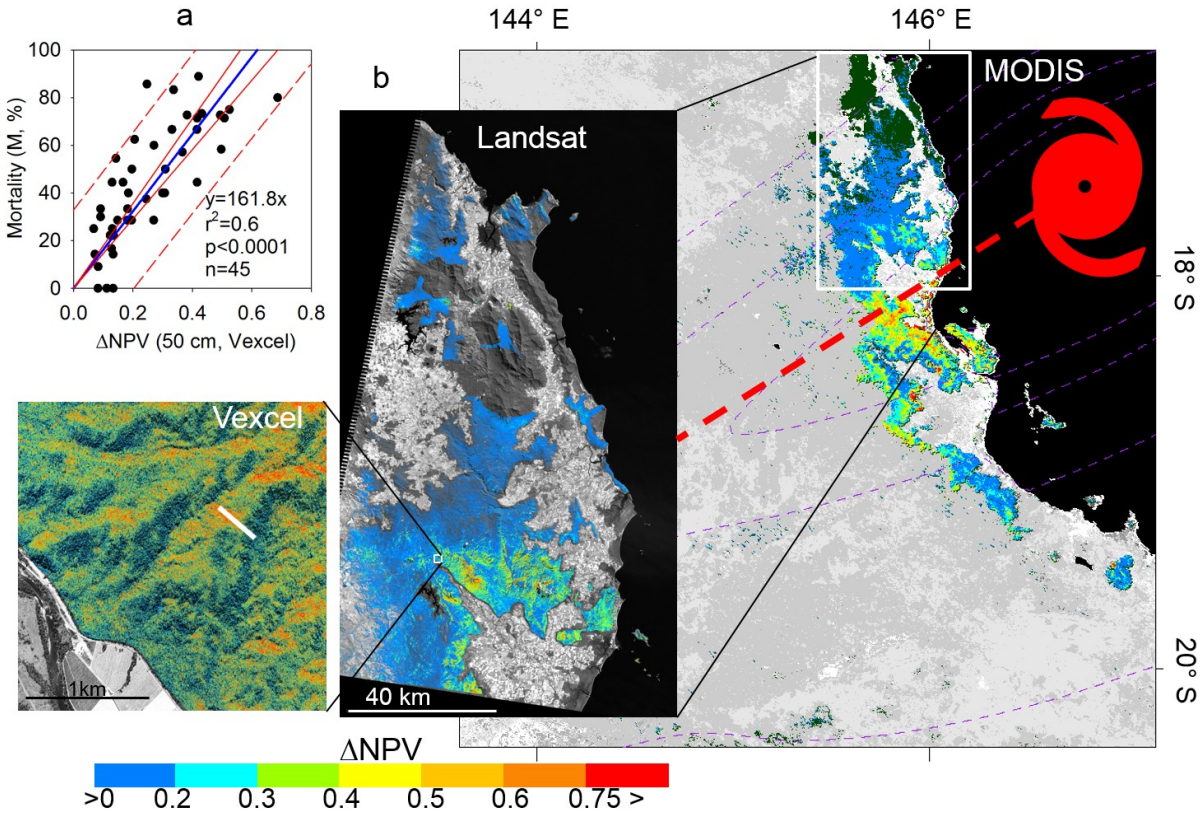

GMTED2010 data was used to determine the surface orientation or aspect, calculated as the direction that a given pixel is facing (0° is north and the angle increase clockwise), slope (0° is the horizontal plane) and surface elevation. Aspect, slope and elevation were calculated using the topographic modeling tool available in ENVI.

This study encompasses areas with Evergreen Broadleaf forests that were affected by Yasi's winds ≥18 m/s (63 km/h).

4. Results

The Vexcel derived disturbance (Vexcel-ΔNPV) correlated significantly ($r^2 = 0.6$, $p < 0.0001$) with the observed tree mortality across the whole gradient of disturbance (Figure 2a). As observed in Figure 2a, we used regression through the origin (RTO) [42] because we normalized the SMA fractions, the ordinary least-squares (OLS) constant was not significant ($p = 0.01$), and the standard errors of the RTO and OLS were very similar. Working in the field presented the following challenges: (*i*) fallen trees occupying the whole plot; (*ii*) fallen trees occupying more than one plot; (*iii*) fallen trees on top of other fallen trees. In spite of the presence of these details the association between Vexcel-ΔNPV and tree mortality was significant. To visualize the location and extent of the different satellite images used (Vexcel, Landsat, MODIS) and the accompanying damage from Yasi, we show ΔNPV maps from these images (Figure 2b). The figure shows that higher disturbances are present in ridges facing the dominant winds (Vexcel-ΔNPV, Landsat-ΔNPV), the effect of wind intensity on disturbance severity at the landscape and regional scale (Landsat-ΔNPV, MODIS-ΔNPV), and maximum disturbance on the left side of the cyclone track (MODIS-ΔNPV). Consistent with the cyclones in the southern hemisphere, Yasi was more severe on the left side of its path. Large regions of unaffected forest (dark green) are found on the right side of the cyclone track (Figure 2b), although this is due to the fact that disturbance was not calculated in these forests because of cloud cover in the pre or post multispectral images. Figure 2b also shows that most of the severe affected areas were impacted by H2 wind speeds (119–153 km/h). Thus, those areas had the highest disturbance severity (high ΔNPV) and consequently presented the highest mortality rates (Figure S3).

Due to their spatial coverage domain and similar spatial resolution GMTED2010 and MODIS-ΔNPV were used to analyze the effect of terrain features on forest disturbance over the whole forested areas impacted by Yasi. Maximum wind speeds from the east-northeast to southwest (80° to 260°) were associated with the observed patterns of disturbance (Figure 3a). The figure shows a concentration of pixels between 80° and 100°, from minimum to maximum ΔNPV values (minimum to maximum disturbance). This forest disturbance was associated with Yasi's track and the onshore flow to the left of the storm track that produced the highest wind speeds (as shown in Figure 3b) and were the main factors of forest disturbance as suggested by the longest spoke (between 80° to 100°) in the wind rose diagram (Figure 3a). In this diagram the length of the spoke is related to the frequency of ΔNPV pixels in a given wind direction, the colors represent the associated ΔNPV values, and the concentric circles represent different frequency (0 is in the origin). Highest disturbance levels were observed: (*i*) in forested areas close to the coast (0 m asl), due to the more intense winds in coastal areas compared to inland areas; (*ii*) on the left side of the cyclone track, where the translation speed enhances the wind; and (*iii*) about 32 km from the track, consistent with the position of the eyewall,

and consistent with tropical cyclone climatology [43]. Figure 3b shows that both wind speed and disturbance severity decrease for locations that experienced peak winds with more of a southerly or westerly component. Large disturbance values were also observed where the wind was strongest and the wind direction had high variability (near the storm center). Figure 3b also shows a group of pixels contouring most of the disturbed pixels. It is related to the higher wind speed that affected coastal areas and to the pattern of forest distribution in the study region (Figure 1).

Figure 3c shows a bimodal pattern of forest disturbance associated with aspect. The first peak was observed on terrain features with aspects of 60°–90° (NE–E), corresponding to surfaces with orientations facing toward the direction of maximum wind speed, and higher slopes. In general, with respect to Yasi's track, land surfaces with aspects varying from 90° ± 30° were found to be highly susceptible to topographic accelerations. A second peak was observed between 150° and 260° which corresponds to upwind areas affected by the dominant winds (Figure 3a). Lowest levels of disturbance was observed in areas with aspects from 260° (west) to ~60° (east) which may be related to the sheltered (lee) sides (with respect to the direction of the strongest winds). In addition, the severity of disturbance decreased on shallower slopes. Thus, ΔNPV decreases with a decrease in slope and an aspect facing off the track of the cyclone or away from the dominant surface winds. As observed in Figure 1, from east to west the study region presents a sequence of forests-land use-forests in a North-South orientation. The first band of forests ranges from 0 to about 600 m asl. The second band of forests ranges from about 300 to 1500 m asl. From the surface level to about 600 m asl both bands of forests were affected by Yasi's winds, but a clear pattern between disturbance and surface elevation is not observed here (Figure 3d), probably due to the overlap of topographic affects from the sequence forests-land use-forests, tree species, soil types, *etc.* [18]. From 600 to 1500 m asl a decrease in disturbance severity with surface elevation is clearly observed (Figure 3d). Figure 3d also shows that for a given surface wind speed, forest disturbance severity increased with elevation. Since H*wind is not sensitive to terrain effects because of its coarse resolution and methodological design, the increase in disturbance with increasing height suggests complex terrain interactions act to speed up wind at higher elevations (consistent with Figure 2b).

In order to assess tree mortality across the entire area impacted by Yasi, successive scaling procedures (Vexcel -Landsat-MODIS) were performed. As observed in Figure 4 the scaling procedure produced a loss of information. Thus, underestimated mortality is expected. Each scaling yielded significant correlations (Figure 4) enabling the calculation of tree mortality as a function only of MOIDS-ΔNPV (Figure S3). Yasi affected a total of 36,278 forested pixels from MODIS ΔNPV, equivalent to ~9000 km^2 of forest. A Monte Carlo simulation, which included the uncertainties of the biomass carbon map (Figure S1) and stem density (Figure S2), as well as the standard errors of the estimated coefficients from the scaling process (field site, Vexcel, Landsat and MODIS), was used to calculate the total number of dead trees and committed carbon loss using 10,000 interactions in forested areas affected by winds ≥18 m/s. Yasi produced a mortality of 302 M ± 80 M (±SD) (M = 10^6) trees representing a committed carbon loss of 65 TgC ± 14 TgC (±SD), equivalent to a large fraction of the net sink of carbon from Australian forest land in 2010 [44].

Figure 3. MODIS-ΔNPV was used to analyze the effect of wind direction and topography across the whole forested area impacted by Yasi's winds ≥18 m/s. (**a**) Winds from the NE to SW impacted forests with maximum forest disturbances (maximum ΔNPV) produced by NE winds; (**b**) Both wind speed and direction influence the severity of disturbance (ΔNPV); (**c**) The effect of surface orientation (aspect) and slope angle on disturbance. ΔNPV and slope angle were binned into 30°-aspect intervals between 0 and 360 (12 bins). For each interval the average was taken and multiplied by a weight value (number of pixel in the bin divided by the number of total pixels) and centered at each aspect bin interval. ΔNPV was finally normalized. (**d**) Association between ΔNPV, surface height and cyclones wind speeds (H*Wind, m/s). Data in (a), (c) and partially (d) are from [18].

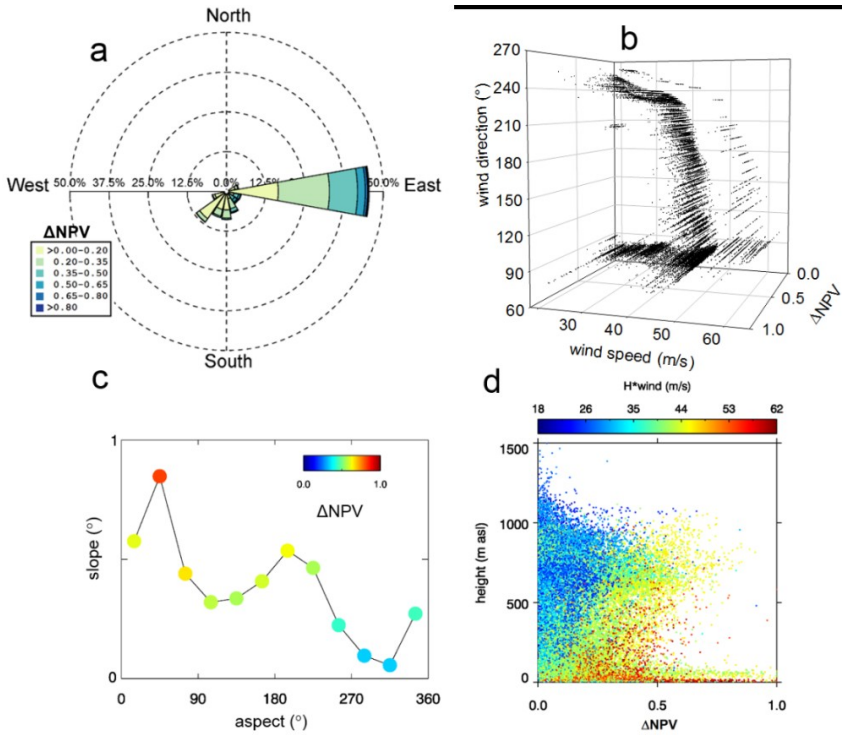

Figure 4. Scaling up from local (**a**) to regional (**b**) derived disturbance. The scaling up was performed by aggregating pixels to the respective pixel size of comparison. The linear regression (blue line), and the 95% confidence (solid red line) and prediction (dashed red line) bands are shown. Data in (b) are from [18].

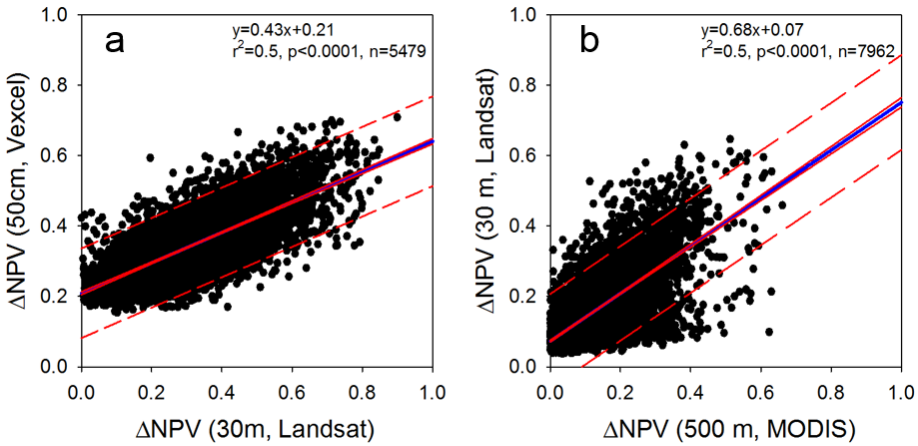

5. Discussion

5.1. Patterns of Forest Disturbance Associated with Topography

Our results show that terrain features are important factors governing the severity of forest damage (Figures 2b and 3b). Our results are in agreement with previous studies [2,10,18,19,45] that indicate that (1) areas with greater directional wind exposure experience the highest levels of damage with slope and aspect being important attributes; and (2) that disturbance decreases with elevation. In addition, specifically for Yasi, we observed that most of the observed disturbance was associated with surfaces having aspects ranging from south (~150°) to west (~260°). To our knowledge no studies examining the relationship between hurricane wind intensity, direction, and topographic position for Yasi have yet been presented. However, winds from south to west are expected as was the case reported for cyclone Larry in 2006 [46] which made landfall in a nearby location, and also moved westward.

Here, MODIS data was used to assess the forest disturbance severity over the whole forested areas affected by Yasi. To facilitate a direct comparison between the disturbance pattern and landforms we used a topographic data comparable to MODIS resolution. This regional assessment would be hard to perform using Landsat due to the necessity of cloud-free imagery and collected at similar times requirements that are hard to meet in tropical rainforested areas associated with intense and frequent convection processes responsible for cloud formation [47].

5.2. Disturbance Severity and Forests Type

The regression equation between field-observed tree mortality and Vexcel-ΔNPV developed in this study can be compared with the equation derived for temperate forests using a similar methodology [17,18] (Figure S4). This study found higher tree mortality in a tropical rainforest than our previous studies over temperate forests [17,18]. The slope of the disturbance metric *versus* tree mortality in tropical forests was about three-fold steeper than the slope found in temperature forests [17,18]. Possible explanations, include the independent or collective effect of: (*i*) an Australian rainforest that is less resistant to hurricane winds due to the lower frequency of hurricane landfalls in comparison with the U.S Gulf Coast (Figure S5) as determined using the IBTrACS data (International Best Track Archive for Climate Stewardship) [48]. However, this data presents many cases of cyclones that made landfall in the Australian rainforests with missing wind speed data. These cases were not included in our analysis; (*ii*) the higher stem density in Australian rainforest resulting in greater collateral damage when trees fall on adjacent trees. The average stem density in the Australian tropical rainforest was found to be about two-fold higher than that found in U.S. Gulf Coast forest ecosystems (Table S1). Thus, stem density may be a key variable that could lead to the development of a universal model to quantify the destructive impacts of hurricanes in different forest ecosystems. Additional field-based data collection is required to confirm the generality of this finding; (*iii*) shallow root system. The higher rainfall in Australia implies a shallow root system that does not provide a strong anchor against strong winds. Independently of the contribution of these factors on cyclone-related tree mortality, it is clear that multispectral data were sensitive to them.

5.3. Assessment of tree Mortality and Committed Carbon

In this study we used tree mortality (uprooted trees) to quantify the interaction of cyclones on ecosystems. Since our quantification of tree mortality relies on field work performed 17 month after Yasi's landfall, our calculations refers to the period of "immediate effect" of cyclones on forest ecosystems. The immediate effect period ranges from landfall to 3 years after landfall [4]. In addition, the SMA analyses presented did not use soil endmember since it was not a significant fraction of imagery. Besides the infrequent occurrence of bare soil, methodologically it is advantageous not to use endmembers that are not actually present everywhere [39].

Our calculation of Yasi impact on the regional carbon balance is illustrative of the magnitude and significance of the potential carbon loss. More accurate quantification would need to consider a range of additional factors such as the immediate reduction of photosynthetic carbon sequestration, rates of decomposition and the countering effects of stimulated leaf flush, accelerated vegetative regrowth and soil carbon dynamics. The importance of these factors was outside the scope of this study and was not considered.

A scaling process was performed in this study. SMA is based on the spectral characteristics of pixels making the scaling possible since Landsat and MODIS are spectrally similar [49,50]. This similarity has allowed, for instance, the MODIS-Landsat data blending [51,52]. This suggests that the main source of uncertainty is the scaling method used. In this study we used the nearest neighbor approach since it appears to yield good results [53] but, as observed, this approach produced underestimates in the coarser resolution. Optimum scaling methodology is an area of current study [54], but ultimately any process is expected to reduce the proportion and value of ΔNPV [55–57], thereby under-estimating overall tree mortality.

Due to warmer sea surface temperatures, cyclones last for a longer period in tropical regions than in temperate regions before dispersing [19]. This characteristic associated with the higher stem density observed in tropical forest have important carbon footprint implications due to the larger amount of carbon stored in tropical rainforests compared to temperate forests [21]. For instance, the forested area affected by Yasi was only half of the forested area affected by hurricane Katrina that hit the U.S. Gulf coast in 2005 [8,17]. However, Yasi produced a tree mortality comparable to that of Katrina.

Tropical cyclone intensity is projected to increase in a warming climate [20] and the effect of these cyclones on tropical rainforests may produce positive feedbacks with climate that could further intensify these projections. Therefore, strategies that protect native rainforests should be adopted [58].

5.4. Uncertainties, Errors, and Accuracy Issues

Our analysis on the sensitivity of multispectral data to forest disturbance in complex terrain is based on data with a spatial resolution of 500 m. Thus the local effects of topography via changes in wind intensity and direction were not considered. These changes were embedded in the coarse resolution of our data. Future studies should address the effect of local topography on disturbance by using a 30 m ASTER Global Digital Elevation Map V2 [59] in concert with Landsat imagery. At this scale, the effects of forest structure as well as tree size and species should be considered since they strongly

affect the disturbance patterns [11,18]. Cyclone wind surface data with similar resolution would be necessary to quantify the effect of topographic accelerations on tree disturbance.

Here we used one set of endmembers to be representative of the whole tropical forested region. While this was a statistically supported approach, it is possible a more accurate disturbance metric could be obtained using multiple sets of endmembers [60].

Tree mortality and committed carbon release calculations were embedded in a Monte Carlo simulation, which included the uncertainties of the biomass carbon map and stem density, as well as the standard errors of the estimated coefficients from the scaling process using 10,000 interactions per disturbed pixel. Means and standard deviations of tree mortality and carbon loss (Figure S3) were then calculated.

6. Conclusions

Our results shown that multispectral data was sensitive to the spectral signature of tree mortality and captured the observed effects of topography on disturbance patterns associated with tropical cyclones in a complex mountainous terrain. By using multispectral data we found that most frequent disturbance was associated with forest located along (±30°) the path of cyclone track. Surface orientation and slope co-vary positively with disturbance with disturbance decreasing with a decrease in slope and an aspect facing off the track of the cyclone or away from the dominant surface winds. Increase in disturbance with surface elevation was also observed. However, areas affected by the same wind intensity presented increased levels of disturbance with increasing elevation suggesting that complex terrain interactions act to speed up wind at higher elevations. The changes in wind direction and intensity produced by complex terrain need more research in order to better understand the effect of cyclones on forest ecosystems. A key component in our study was the cyclone wind field. Our study is the first to use the Hurricane Research Division of the National Oceanic and Atmospheric Administration (HRD/NOAA) Real-time Hurricane Wind Analysis System (H*wind) system in the southern Hemisphere. However, as noticed before, more work is needed in order to produce more detailed H*wind data. Integrating multispectral data with high resolution cyclone surface wind data to quantify cyclone induced forest disturbance will improve forest management strategies and produce reliable models of tree disturbance and carbon loss associated with cyclones.

Acknowledgments

We thank the four anonymous reviewers and one External editor for their valuable comments on our manuscript. Funding from a NASA-IDS (NNX10AP11G) grant to the University of Maryland with a subcontract to Tulane University, and DOE's Office of Biological and Environmental Research (Contract No. DE-AC02- 05CH11231), under the Climate and Earth System Modeling Program, supported the work presented here. The authors also thank to Sonya Jeffrey, Douglas Jeffrey and Ernie Grant (INGAN Pty Ltd, http://www.ingan.com.au) and to Mr. Noel and Mrs. Dot Barrow (A Tropical Scape B&B, http://www.atropicalescape.com/) for all the logistic support. RINJ thank the Office of Biological and Environmental Research of the U.S. Department of Energy as part of their Regional and Global Climate Modeling (RGCM) Program.

Author Contributions

All authors contributed extensively to the work. Robinson Negrón-Juárez, Jeffrey Chambers and George Hurtt designed and performed the experiment. Bachir Annane, Stephen Cocke, and Mark Powell produced the H*wind data and contributed significantly to the analysis, interpretation and discussion of results. Stephen Goosem, Michael Stott, Daniel J. Metcalfe and Sassan S. Saatchi provided the ecological data and contributed significantly to the analysis, interpretation and discussion of results. Robinson Negrón-Juárez wrote the manuscript. Stephen Goosem edited the manuscript.

Conflicts of Interest

The author declares no conflict of interest.

References

1. World Meteorological Organization. Available online: http://www.wmo.int, tropical cyclones (accessed on 5 December 2013).
2. Foster, D.; Boose, E. Patterns of forest damage resulting from catastrophic wind in central New England, U.S.A. *J. Ecol*. **1992**, *80*, 79–98.
3. Metcalfe, D.; Bradford, M.; Ford, A. Cyclone damage to tropical rain forests: Species- and community-level impacts. *Austral Ecol*. **2008**, *33*, 432–441.
4. Lugo, A. Visible and invisible effects of hurricanes on forest ecosystems: An international review. *Austral Ecol*. **2008**, *33*, 369–398.
5. Everham, E.; Brokaw, N.V. Forest damage and recovery from catastrophic wind. *Bot. Rev*. **1996**, *62*, 113–185.
6. Van Bloem, S.; Murphy, P.; Lugo, A.; Ostertag, R.; Costa, M.; Bernard, I.; Colon, S.; Mora, M. The influence of hurricane winds on Caribbean dry forest structure and nutrient pools. *Biotropica* **2005**, *37*, 571–583.
7. Turton, S. Landscape-scale impacts of Cyclone Larry on the forest of northern Australia, including comparisons with previous cyclones impacting the region between 1858 and 2006. *Austral Ecol*. **2008**, *33*, 409–416.
8. Chambers, J.; Fisher, J.; Zeng, H.; Chapman, E.; Baker, D.; Hurtt, G. Hurricane Katrina's carbon footprint on U.S. Gulf Coast forest. *Science* **2007**, *318*, doi: 10.1126/science.1148913.
9. Negrón-Juárez, R.; Chambers, J.; Zeng, H.; Baker, D. Hurricane driven changes in land cover create biogeophysical climate feedbacks. *Geophys. Res. Lett*. **2008**, *35*, doi:10.1029/2008GL035683.
10. Boose, E.; Serrano, M.; Foster, D. Landscape and regional impacts of hurricanes in Puerto Rico. *Ecol. Monogr*. **2004**, *74*, 335–352.
11. Xi, W.; Peet, R.; Decoster, J.; Urban, D. Tree damage risk factors associated with large, infrequent wind disturbances of Carolina forests. *Forestry* **2008**, *81*, 317–334.
12. Masek, J.; Huang, C.; Wolfe, R.; Cohen, W.; Hall, F.; Kutler, J.; Nelson, P. North American forest disturbance mapped from a decadal Landsat record. *Remote Sens. Environ*. **2008**, *112*, 2914–2926.

13. Frolking, S.; Palace, M.; Clark, D.; Chambers, J.; Shugart, H.; Hurtt, G. Forest disturbance and recovery: A general review in the context of spaceborne remote sensing of impacts on aboveground biomass and canopy structure. *J. Geophys. Res*. **2009**, *114*, 1–27.
14. Huang, C.; Goward, S.N.; Masek, J.G.; Thomas, N.; Zhu, Z.; Vogelmann, J.E. An automated approach for reconstructing recent forest disturbance history using dense Landsat time series stacks. *Remote Sens. Environ*. **2010**, *114*, 183–198.
15. Kennedy, R.E.; Yang, Z.; Cohen, W.B. Detecting trends in forest disturbance and recovery using yearly Landsat time series: 1. LandTrendr—Temporal segmentation algorithms. *Remote Sens. Environ*. **2010**, *114*, 2897–2910.
16. Zhu, Z.; Woodcock, C.E.; Olofsson, P. Continuous monitoring of forest disturbance using all available Landsat imagery. *Remote Sens. Environ*. **2012**, *122*, 75–91.
17. Negrón-Juárez, R.; Baker, D.; Zeng, H.; Henkel, T.; Chambers, J. Assessing hurricane-induced tree mortality in U.S. Gulf Coast forest ecosystems. *J. Geophys. Res. Biogeo*. **2010**, *115*, doi:10.1029/2009JG001221.
18. Negrón-Juárez, R.; Baker, D.; Chambers, J.; Hurtt, G.; Goosem, S. Multi-scale sensitivity of Landsat and MODIS to forest disturbance associated with tropical cyclones. *Remote Sens. Environ*. **2014**, *140*, 679–689.
19. Boose, E.; Foster, D.; Fluet, M. Hurricane impacts to tropical and temperate forest landscapes. *Ecol. Monogr*. **1994**, *64*, 369–400.
20. Intergovernmental Panel on Climate Change. Climate Change 2007: The Physical Science Basis. In *Contribution of Working Group I to the Fourth Assessment Report of the Intergovernmental Panel on Climate Change*; Solomon, S., Qin, D., Manning, M., Chen, Z., Marquis, M., Averyt, K.B., Tignor, M., Miller, H.L., Eds.; Cambridge University Press: New York, NY, USA, 2007.
21. Saatchi, S.; Harrys, N.; Brown, S.; Lefsky, M.; Mitchard, E.; Salas, W.; Zutta, B.; Buemann, W.; Lewis, S.; Hagen S.; *et al.* Benchmark map of forest carbon stock in tropical regions across three continents. *Proc. Natl. Acad. Sci. USA* **2011**, *108*, 9899–9904.
22. The Saffir-Simpson Hurricane Wind Scale. Available online: http://www.nhc.noaa.gov/pdf/sshws.pdf (accessed on 5 December 2013).
23. Severe Tropical Cyclone Yasi—Bureau of Meteorology. Available online: http://www.bom.gov.au/cyclone/history/yasi.shtml (accessed on 5 December 2013).
24. Webb, L. Cyclones as an ecological factor in tropical lowland rainforest, North Queensland. *Aust. J. Bot*. **1958**, *6*, 220–228.
25. Wet Tropics Management Authority—Wet Tropics World Heritage Area. Available online: http://www.wettropics.gov.au (accessed on 5 December 2013).
26. Metcalfe, D.; Ford, A. Floristic Biodiversity in the Wet Tropics. In *Chapter 7 in Living in a Dynamic Tropical Forest Landscape*; Stork, N., Turton, S., Eds.; Blackwell: Oxford, UK, 2008; pp. 123–132.
27. Metcalfe, D.; Ford, A. A re-evaluation of Queensland's Wet Tropics based on primitive plants. *Pac. Conserv. Biol*. **2009**, *15*, 80–86.
28. Goosem, S.; Morgan, G.; Kemp, J. Wet Tropics. In *The Conservation Status of Queensland's Bioregional Ecosystems*; Sattler, P.S., Williams, R.D., Eds.; Environmental Protection Agency: Brisbane, Australia, 1999; pp. 7/1–7/73.

29. Powell, M.D.; Houston, S.; Amat, L.; Morisseau-Leroy, N. The HRD real-time hurricane wind analysis system. *J. Wind Eng. Ind. Aerodyn*. **1998**, *77–78*, 53–64.
30. Powell, M.D.; Murillo, S; Dodge, P.; Uhlhorn, E.; Gamache, J.; Cardone, V.; Cox, A.; Otero, S.; Carrasco, N.; Annane, B.; Fleur, R. Reconstruction of Hurricane Katrina's wind fields for storm surge and wave hindcasting. *Ocean Eng*. **2010**, *37*, 26–36.
31. Yasi H*Wind Data. Available online: ftp://ftp.aoml.noaa.gov/hrd/pub/annane/Yasi (accessed on 5 December 2013).
32. AEROmetrex. Available online: http://aerometrex.com.au (accessed on 5 December 2013).
33. Dimap Australia. Available online: http://www.dimap.com.au (accessed on 5 December 2013).
34. U.S. Geological Survey. Available online: http://calval.cr.usgs.gov (accessed on 5 December 2013).
35. Vermote, E.; Kotchenva, S. Atmospheric correction for the monitoring of land surfaces. *J. Geophys. Res*. **2008**, *113*, doi:10.1029/2007JD009662.
36. Souza, C.; Roberts, D.; Cochrane, M. Combining spectral and spatial information to map canopy damage from selective logging and forest fires. *Remote Sens. Environ*. **2005**, *98*, 329–343.
37. NASA Land Data Products and Services-U.S. Geological Survey. Available online: https://lpdaac.usgs.gov (accessed on 5 December 2013).
38. Adams, J.; Sabol, D.; Kapos, V.; Almeida Filho, R.; Roberts, D.; Smith, M.; Gillespie, A. Classification of multispectral images based on fractions of endmembers: Application to land-cover change in the Brazilian Amazon. *Remote Sens. Environ*. **1995**, *53*, 137–154.
39. Adams, J.B.; Gillespie. A.R. Remote Sensing of Landscapes with Spectral Images. In *A Physical Modeling Approach*; Cambridge University Press: Cambridge, UK, 2006.
40. Boardman, J.; Kruse, F.; Green, R. Mapping Target Signatures via Partial Unmixing of AVIRIS Data. In Proceedings of Fifth Annual JPL Airborne Earth Science Workshop, Pasadena, CA, USA, 23–26 January 1995; pp. 23–26.
41. Chambers, J.Q.; Higuchi, C.; Schimel, J.; Fererira, L.; Melack, J. Decomposition and carbon cycling of dead trees in tropical forests of the central Amazon. *Oecologia* **2000**, *122*, 380–388.
42. Eisenhauer, J. Regression through the Origin. *Teach. Stat.* **2003**, *25*, 76–80.
43. Houze, R. Clouds in tropical cyclones. *Mon. Weather Rev*. **2010**, *138*, 293–344.
44. Commonwealth of Australia, National Inventory Report-NIR 2010. Available online: http://climatechange.gov.au/sites/climatechange/files/documents/03_2013/national-inventory-report-2010–2.pdf (accessed on 29 January 2014).
45. Brokaw, N.; Walker, L. Summary of the effects of Caribbean hurricanes on vegetation. *Biotropica* **1991**, *23*, 442–447.
46. Ramsay, H.; Leslie, L. The effects of complex terrain on severe landfalling tropical Cyclone Larry (2006) over Northeast Australia. *Mon. Weather Rev*. **2008**, *136*, 4334–4354.
47. Asner, G.P. Cloud cover in Landsat observations of the Brazilian Amazon. *Int. J. Remote Sens*. **2001**, *22*, 3855–3862.
48. Knapp, K.; Kruk, M.; Levinson, D.; Diamond, H.; Neumann, C. The International Best Track Archive for Climate Stewardship (IBTrACS): Unifying tropical cyclone best track data. B. *Am. Meteorol. Soc*. **2010**, *91*, 363–376.

49. Gao, F.; Masek, J.; Schwaller, M.; Hall, F. On the blending of the Landsat and MODIS surface reflectance: Predicting daily Landsat surface reflectance. *IEEE Trans. Geosci. Remote Sens*. **2006**, *44*, 2207–2218.
50. Justice, C.O.; Townshend, J.R.G.; Vermote, E.F.; Masuoka, E.; Wolfe, R.E.; Saleous, N.; Roy, D.P.; Morisette, J.T. An overview of MODIS Land data processing and product status. *Remote Sens. Environ.* **2002**, *83*, 3–15.
51. Roy, D.P.; Ju, J.; Lewis, P.; Schaaf, C.; Gao, F.; Hansen, M.; Lindquist, E. Multi-temporal MODIS–Landsat data fusion for relative radiometric normalization, gap filling, and prediction of Landsat data. *Remote Sens. Environ.* **2008**, *112*, 3112–3130.
52. Hilker, T.; Wulder, M.A.; Coops, N.C.; Seitz, N.; White, J.C.; Gao, F.; Masek, J.G.; Stenhouse, G. Generation of dense time series synthetic Landsat data through data blending with MODIS using a spatial and temporal adaptive reflectance fusion model. *Remote Sens. Environ.* **2009**, *113*, 1988–1999.
53. Hubert, S.; Schwarzer, S.; Jaquet, J.M. Spatial degradation of classified satellite images. *Open Remote Sens. J.* **2012**, *5*, 64–72.
54. Arun, P.V.; Katiyar, S.K. Intelligent adaptive resampling technique for the processing of remotely sensed imagery. *Ann. GIS* **2014**, *20*, 53–60.
55. Gupta, R.; Prassad, T.; Rao, P.; Manikavelu, B. Problems in upscaling of high resolution remote sensing data to coarse spatial resolution over land surface. *Adv. Space Res*. **2000**, *27*, 1111–1121.
56. Fisher, J.; Mustard, J. Cross-scalar satellite phenology from ground, Landsat and MODIS data. *Remote Sens. Environ*. **2007**, *109*, 261–273.
57. Roman, M.; Gateve, C.; Shuai, Y.; Wang, Z.; Gao, F.; Masek, J.; He, T.; Liang, S.; Schaaf, C. Use of *in situ* and airborne multiangle data to assess MODIS- and Landsat-based estimates of directional reflectance and albedo. *IEEE Trans. Geosci. Remote Sens.* **2013**, *51*, 1393–1404.
58. Turton, S. Securing landscape resilience to tropical cyclones in Australia's wet tropics under a changing climate: lessons from cyclones Larry (and Yasi). *Geogr. Res*. **2012**, *50*, 15–30.
59. Aster GEM-NASA. Available online: http://asterweb.jpl.nasa.gov/gdem.asp (accessed on 5 December 2013).
60. Roberts, D.; Gardner, M.; Church, R.; Ustin, S.; Scheer, G.; Green, R. Mapping chaparral in the Santa Monica Mountains using multiple endmember spectral mixture models. *Remote Sens. Environ*. **1998**, *65*, 267–279.